A new discrete model to better consider tracer distribution along boreholes during the Finite Volume Point Dilution Method

Nataline Simon[1], Serge Brouyère[1] and Pierre Jamin[1,2]

[1] Department Urban and Environmental Engineering, Hydrogeology and Environmental Geology, University of Liege, Building B52, 4000 Sart Tilman, Belgium

[2] Nagaré Tech, University of Liege, Aquapôle, Building B53, 4000 Sart Tilman, Belgium

Corresponding authors: Nataline Simon (nataline.simon@uliege.be); Serge Brouyère (Serge.Brouyere@uliege.be)

Highligths

- For non-perfect mixing conditions, classical FVPDM overestimates groundwater fluxes
- A new discrete model considering the recirculation flow rate is introduced
- The new model allows simulating the tracer distribution along the well axis
- Providing better estimates of groundwater fluxes

Abstract

The Finite Volume Point Dilution Method (FVPDM) is a single-well tracer experiment which has been successfully used in many hydrogeological contexts to quantify groundwater fluxes. During continuous injection of tracer into a well, the tracer concentration evolution measured within the tested well directly depends on the groundwater flow crossing the well screens. Up to now, the FVPDM mathematical formulation used to simulate the tracer concentration evolution measured in the tested well assumed perfect homogenization of the tracer along the tested interval, which is a reasonable assumption in many cases. However, when FVPDM are performed in long-screened boreholes or in very permeable aquifer materials, the recirculation flow rate imposed to ensure mixing is suspected to be too low to perfectly homogenize the tracer. In order to assess the effect of non-perfect mixing on FVPDM results, we introduce here a new discrete model that explicitly considers the recirculation flow rate. The mathematical developments are validated using field measurements, and a sensitivity analysis is proposed to assess the effect of the mixing flow rate on tracer concentration homogenization within the well. Results confirm that, when the recirculation flow rate applied is not high enough compared to the groundwater flow rate, the tracer distribution is not uniform in the tested interval. In this case, the use of the classical analytical solution, commonly used to

interpret the concentration evolution leads to highly overestimated groundwater fluxes. The discrete model introduced here can be used instead to properly estimate groundwater fluxes and assess the tracer distribution within the tested interval. The discrete model offers the possibility of interpreting field measurements conducted under non-perfect mixing conditions and increases the range of fluxes that can be investigated through FVPDM.

Keywords

Finite Volume Point Dilution Method ; Non-Perfect Mixing; Improved FVPDM model; Tracer Distribution within the well;

Nomenclature

Experiment parameters			*Discretized domain*		
r_w	Inner radius of the well	[L]	Δz	Vertical size	[L]
e_{scr}	Well screen length	[L]	Nz	Number of elementary cells Δz_i	[-]
h_w	Height of the water column	[L]	Δt	Calculation time step	[T]
V_w	$= \pi r_w^2 h_w$, water volume in the well	[L^3]	Nt	Number of elementary cells Δt_j	[-]
Q_{recirc}	Recirculation rate (or mixing flow rate)	[L^3T^{-1}]	j	Subscript indicating that the corresponding quantity is evaluated at $t=t_j$ *j= 1,2,…,Nt*	[-]
Q_{inj}	Injection rate	[L^3T^{-1}]	Nz_{scr}	Number of elementary cells Δz_i in the screened section	[-]
Tracer concentration					
C_{inj}	Tracer concentration in the injection solution	[M L^{-3}]	i	Subscript *i= 1,2,…,Nz*	[-]
C_w	Tracer concentration in the water	[M L^{-3}]	τ_i	Time required for the tracer to reach depth z_i	[T]
C_0	Tracer concentration in the aquifer and within the well at initial time	[M L^{-3}]	*Non-dimensional formulations* $C^* = \frac{C}{C_{inj}}$ $Q^* = \frac{Q}{Q_{cr}}$		
Flow parameters			$t_i^* = {t - \tau_i}/{T_{wi}}$		
q_d	Effective Darcy flux in the aquifer	[L T^{-1}]			
α_w	Distortion coefficient	[-]			
q_{app}	$= \alpha_w q_d$, Apparent Darcy flux in the borehole	[L T^{-1}]	T_w	Time needed to replace the water at the critical injection rate	[T]
Q_t	$= 2\, r_w e_{scr} q_{app}$, transit flow rate under ambient conditions	[L^3T^{-1}]			
Q_{cr}	$= \pi Q_t$, critical injection rate	[L^3T^{-1}]			
Q_t^{in}	Transit flow rate under injection conditions	[L^3T^{-1}]			

1. Introduction

Characterizing groundwater fluxes is essential in many hydrogeological studies, especially to understand contaminant transport and behavior, to investigate groundwater/surface water interactions or else in geothermal applications and in geotechnical engineering. In this context, tracer dilution tests have been widely developed and applied to quantify groundwater fluxes (Hall, 1993; Novakowski et al., 1995, 2006; West and Odling, 2007; Drost et al., 1968; Lewis et al., 1966; Pitrak et al., 2007; Hatfield et al., 2004; Halevy et al., 1967). Among single-well techniques, the Finite Volume Point Dilution Method (FVPDM), that is a generalization of classical point dilution tests, was developed and validated (Brouyère, 2003; Brouyère et al., 2008). FVPDM tests are performed by continuously injecting a tracer into the well (at the top of the well or of the tested interval) and monitoring the evolution of the tracer concentration into the same well (Figure 1). The water within the tested interval is continuously mixed through a mixing pump ensuring a homogeneous distribution of the tracer within the tested interval. By doing so, the water is extracted with a pump placed at the bottom of the tested interval and reinjected at the top of the tested interval. During the experiment, the tracer concentration within the well first increases before stabilizing and reaching a plateau. Brouyère et al. (2008) demonstrated that the tracer concentration evolution (and stabilization) depends on the concentration of the injected water (C_{inj}), on the tracer injection flow rate (Q_{inj}) and on the flow rate of the groundwater crossing the screen of the injection well (Q_t^{in}). A part of the injected tracer is carried out of the well by the groundwater flow. Therefore, the higher the groundwater fluxes, the higher the tracer dilution and the lower the tracer concentration remaining in the well.

Measured concentrations can be easily reproduced using the analytical solution introduced by Brouyère et al. (2008) by calibrating the only unknown parameter at steady-state (when concentration is stabilized) : the Darcy flux in the aquifer. The application of FVPDM in many hydrogeological contexts – to characterize groundwater/surface water interactions (Dujardin et al., 2014), fractured aquifer (Jamin et al., 2015), permafrost zone (Jamin et al., 2020), complex sandy aquifer (Goderniaux et al., 2010; Brouyère et al., 2008) or shallow alluvial aquifers (Wildemeersch et al., 2014) – demonstrated the robustness and reliability of the method to provide accurate groundwater fluxes estimates. In addition, since the tracer concentration is sensitive to changes in groundwater flow, the method was also successfully applied under transient groundwater flow conditions (Jamin and Brouyère, 2018; Jamin et al., 2020, 2015).

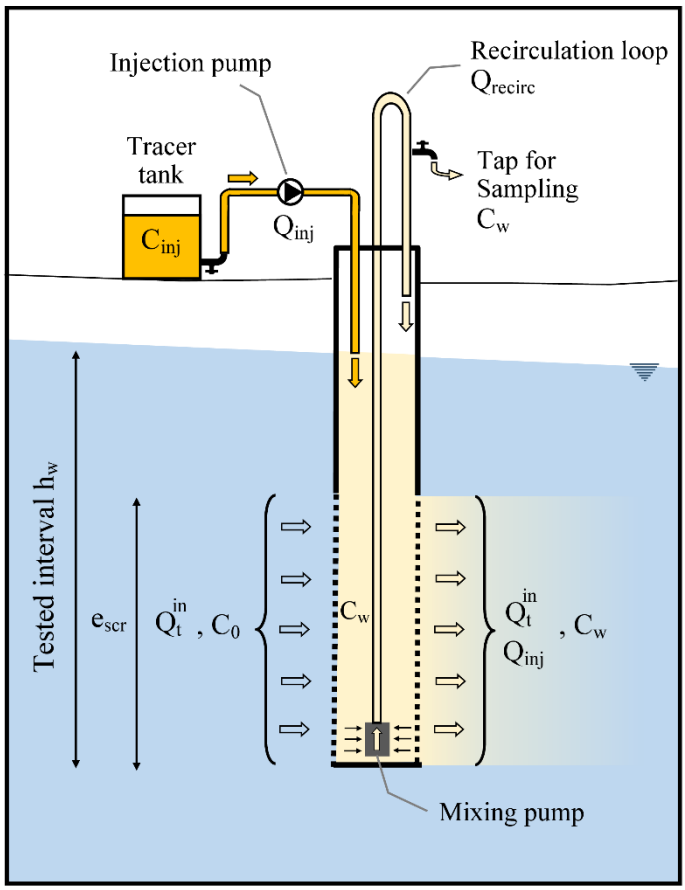

Figure 1. Principle of the FVPDM method (modified from Brouyère et al. (2008))

Analytical and numerical solutions classically used to interpret FVPDM tests (Brouyère, 2003; Brouyère et al., 2008; Jamin and Brouyère, 2018) and to model the tracer concentration evolution within the tested interval (h_w in Fig. 1) rely on the assumption that the mixing flow rate is high enough to ensure a uniform repartition of the tracer mass in the water column. In practice, it can be technically difficult to apply a mixing rate high enough to make sure the tracer concentration is homogenous in the well, as observed by Jamin and Brouyère (2018) who performed FVPDM tests under pumping conditions in a high hydraulic conductivity aquifer. They observed a nonlinear evolution of the groundwater flux with the pumping rate suggesting that the mixing flow rate applied during the experiment was too low compared to the groundwater transit flow rate (passing through the well screen). Their results suggested that under high groundwater transit flow rate, a significant portion of tracer may be carried out of the well before reaching the mixing pump located at the bottom of the tested interval. Therefore, in case of non-perfect mixing, higher tracer concentrations may be found at the top of the tested interval than at the bottom. Such issues are suspected to appear when FVPDM are conducted in long-screened wells, in very permeable aquifer materials or else in fractured or heterogeneous aquifer, as it has been observed for other tracer dilution tests (Poulsen et al., 2019).

Yet, the question of the effect of the mixing flow rate (or recirculation flow rate) on tracer concentration distribution within the tested interval has never been assessed until now. In this context, we introduce here a new discrete FVPDM model which allows simulating tracer concentration profiles in depth along the tested interval. Contrary to classical solutions commonly used to interpret FVPDM tests (Brouyère et al., 2008), this discrete model explicitly considers the recirculation flow rate, which allows assessing the distribution of tracer concentration along the tested interval. This aims to assess the influence of this parameter on the tracer distribution along the tested interval and to propose a solution to interpret FVPDM tests performed under non-perfect mixing conditions.

In the next sections, the new discrete FVPDM model developed to simulate tracer concentration profiles depending on mixing flow rate is introduced. Then, we rely on field data to illustrate the adequacy and relevance of the discrete model to interpret FVPDM results and quantify groundwater fluxes. In the end, a sensitivity analysis is proposed in order to assess the effect of the mixing flow rate on tracer concentration homogenization within the well and on the estimation of groundwater flux using the FVPDM method.

2. Material & Methods

2.1. Presentation of the discrete model

The analytical solution classically used to interpret FVDPM tests, developed by Brouyère et al. (2008), relies on a model based on mass balance equations. Their approach consisted of considering that the variation of tracer mass (and thus concentration) measured over time within the whole tested interval (Figure 1) depends on the tracer mass entering within the tested interval and on the tracer mass leaving the interval. For the discrete model introduced in this paper, a similar approach is developed expect that the tested interval is discretized into a multitude of elementary cells. Thus, the mass balance approach is applied for each cell, which allows simulating the tracer concentration evolution in each cell and provides tracer concentration profiles. Moreover, contrary to the “classical” solution/approach (this term refers to the approach developed by Brouyère et al. (2008) from now), the discrete model is built to take into account the mixing applied within the interval which means that the recirculation flow rate is integrated in mass balance equations.

2.1.1. Discrete Numerical Model

For the discrete model developed here, the domain (the volume of water) is discretized into i elementary cells with vertical size Δz_i (i=1, 2, …, Nz) as shown in Figure 2a. Time is discretized into Nt time steps Δt (j=1,2,…,Nt). Mass balance equations are written for each elementary cell considering that the mass of tracer changes over time depending on flow rates entering and leaving the cell i and on their respective concentrations in tracer.

The approach consists in defining, for each cell, entering and leaving flow rates. To do so, space is divided into two parts: the screened interval discretized into Nz_{scr} cells and the tube interval (no screens) discretized into $Nz\text{-}N_{zscr}$ cells (Figure 2a). This allows considering the effective geometry of the well and adapting the model for each experimental setup.

In the tube interval (Figure 2a, b and c), only vertical flow circulation occurs, meaning that flow rate terms accounting for water and solute transport within the tubewell are the injection flow rate Q_{inj} and the recirculation flow rate Q_{recirc} (ensured by the mixing pump in the bottom of the tested interval). In the screened interval (Figures 2a, d and e), besides the recirculation flow rate, flow rate terms include exchanges between the well and the test aquifer system (transit flow rate). Thus, the transit flow rate $Q_{t,i}^{in}$ corresponding to the flow crossing the well under injection conditions for each interval i is included in the mass balance equations. The detailed mass balance equations written for each cell are detailed in Appendix A.

Once mass balance equations are defined, it is possible to numerically evaluated each equation through the forward difference expression approximant of Δt (Appendix A). Then, the concentration of tracer C_w can be calculated for each cell and each time step $C_{w,i}^{j}$. The initial conditions are $C_{w,i}^{1} = C_0$ (the tracer concentration at j = 1 corresponds to the tracer concentration in the aquifer and in the well at initial time, before tracer injection).

The tracer concentration evolution at top of the well (i = 1), where the tracer injection takes place (Fig. 2b), can be modelled following:

$$V_{wi}C_{\mathrm{w},1}^{j+1} = V_{wi}C_{\mathrm{w},1}^{j} + \left[Q_{recirc}\, C_{w,Nz}^{j-1} - Q_{recirc}\, C_{\mathrm{w},1}^{j} + Q_{inj}C_{inj} - Q_{inj}C_{\mathrm{w},1}^{j}\right]\Delta t \qquad (1)$$

With V_{wi} is the volume of each cell and given by $V_{wi} = \pi r_w^2\, \Delta z$, with r_w the inner radius of the well. C_{inj} corresponds to the tracer concentration in the injection water (tracer tank in

Figure 1) and $C_{w,Nz}^{j-1}$ corresponds to the tracer concentration in the water pumped in the bottom of the well (i = Nz) at j-1 and reinjected in its top at j.

Then, the tracer concentration evolution within the tube interval for i > 2 (Fig. 2c) is modelled following:

$$V_{wi}C_{\mathrm{w,i}}^{j+1} = V_{wi}C_{\mathrm{w,i}}^{j} + \left[Q_{recirc}\, C_{\mathrm{w},i-1}^{j} - Q_{recirc}\, C_{\mathrm{w,i}}^{j} + Q_{inj}C_{\mathrm{w},i-1}^{j} - Q_{inj}C_{\mathrm{w,i}}^{j}\right]\Delta t \qquad (2)$$

At the top of the screened interval (Fig. 2d), the tracer concentration evolution is given by:

$$\begin{aligned} V_{wi}C_{\mathrm{w,i}}^{j+1} = {} & V_{wi}C_{\mathrm{w,i}}^{j} \\ & + \left[Q_{recirc}\, C_{\mathrm{w},i-1}^{j} - Q_{recirc}\, C_{\mathrm{w,i}}^{j} + Q_{t}^{in}{}_{,i}C_0 - Q_{t}^{in}{}_{,i}C_{\mathrm{w,i}}^{j} + Q_{inj}C_{\mathrm{w},i-1}^{j}\right. \\ & \left. - Q_{inj,i}C_{\mathrm{w,i}}^{j} - (Q_{inj} - Q_{inj,i})C_{\mathrm{w,i}}^{j}\right]\Delta t \end{aligned} \qquad (3)$$

And elsewhere in the screened interval (Fig. 2e) by:

$$\begin{aligned} V_{wi}C_{\mathrm{w},i}^{j+1} = {} & V_{wi}C_{w,i}^{j} \\ & + \left[Q_{recirc}\, C_{\mathrm{w},i-1}^{j} - Q_{recirc}\, C_{\mathrm{w},i}^{j} + Q_{t,i}^{in}\, C_0 - Q_{t,i}^{in}\, C_{\mathrm{w},i}^{j} + Q_{inj,\,i-1}\, C_{\mathrm{w},i-1}^{j}\right. \\ & \left. - Q_{inj,i}\, C_{\mathrm{w,i}}^{j} - (Q_{inj,i-1} - Q_{inj,i})C_{\mathrm{w},i}^{j}\right]\Delta t \end{aligned} \qquad (4)$$

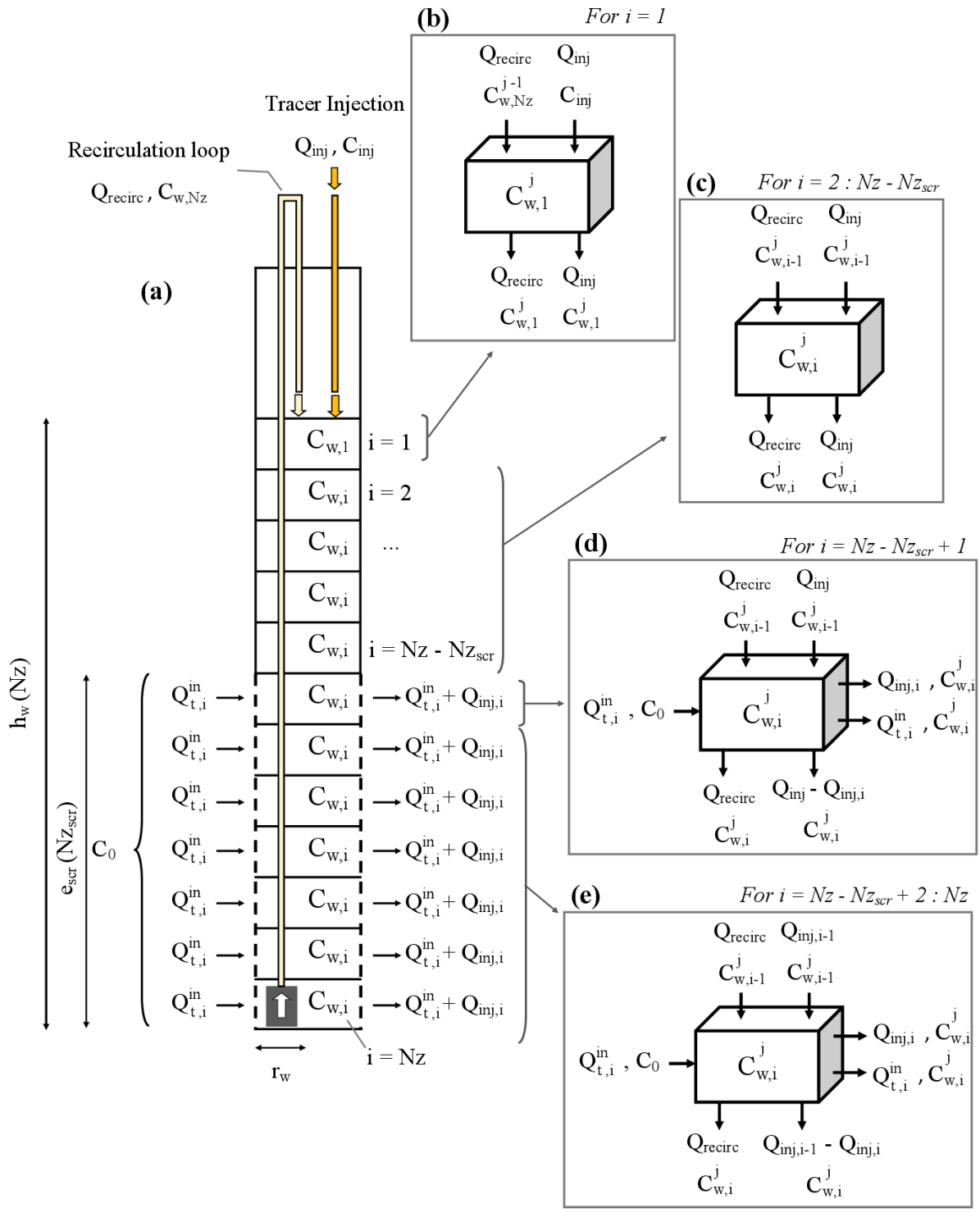

Figure 2. Scheme of the discrete model. In this new approach, the tested well is discretized into i cells (a) and mass balance equations are applied depending on flow rates and their respective tracer concentrations entering and leaving each cell (b,c,d and e).

2.1.2. Flow rates in the screened interval

In the screened interval (Figure 2a), the injection flow rate is distributed along the screen according to the distribution of flow transiting along the screen under ambient conditions ($Q_{t,i}$).

Here, in order to study the mixing within the well, homogeneous flow conditions are assumed along the screen, which means that the portion $Q_{inj,i}$ of the total injection flow rate leaving the screen is calculated following:

$$Q_{inj,i} = \frac{Q_{inj}}{N z_{scr}} \tag{5}$$

Brouyère (2003) proposed a solution to calculate the transit flow rate Q_t^{in} crossing the well screen under injection conditions. Here, instead of calculating the transit flow rate over the tested interval (Brouyère, 2003), the transit flow rate under injection conditions is calculated for each cell i :

$$Q_{t,i}^{in} = \frac{Q_{cr,i}}{\pi} \sin\left(\arccos\left(\frac{Q_{inj,i}}{Q_{cr,i}}\right)\right) - \frac{Q_{inj,i}}{2\pi}\left(2\arccos\left(\frac{Q_{inj,i}}{Q_{cr,i}}\right)\right) \tag{6}$$

The transit flow rate depends on the importance of the injection rate compared to the critical injection rate Q_{cr}. The term Q_{cr} corresponds to the injection rate above which the transit flow rate Q_t is cancelled (radially diverging flow prevails), making the flow estimation impossible (Brouyère et al., 2008). Q_{cr} is calculated for each cell i following:

$$Q_{cr,i} = \pi\, Q_{t,i} = 2\pi\, r_w\, \Delta z\, q_{app,i} \tag{7}$$

with $q_{app,i}$ the apparent Darcy flux measured for each interval Δz. The estimation of the effective Darcy flux q_d in the aquifer requires evaluating the value of flow distortion coefficient α_w (Drost et al., 1968; Brouyère, 2003), that expresses the ratio between the apparent water flow rate crossing the screen section and the theoretical (or effective) flow rate that would transit across the same section in the absence of the well ($q_{app} = \alpha_w q_d$). In this study, we focus on estimating the apparent Darcy flux, also called the apparent groundwater flux.

2.1.3. Space discretization

The numerical scheme (Equation A-**Erreur ! Source du renvoi introuvable.**) is applicable when the Courant-Friedrich-Levi (CFL) stability condition is satisfied. It requires that sizes of Δz and Δt have to be fixed so that the non-dimensional Courant Number Cr does not exceed 1. Here, Cr is expressed as:

$$Cr = \frac{Q_{recirc}}{\pi r_w^2}\frac{\Delta t}{\Delta z} < 1 \tag{8}$$

With the ratio $Q_{recirc}/\pi r_w^2$ accounting for the vertical flow velocity into the well.

2.1.4. Tracer distribution along the screened interval

In the case of perfect mixing, the tracer distribution is homogeneous all along the tested interval. In contrast, for the case of non-perfect mixing, lower tracer concentrations are expected at the bottom of the tested interval. Thus, the ratio of concentrations between the bottom and the top of the tested interval, called $R_{b/t}$, can be used to assess the importance of tracer concentration gradient within the interval. When the ratio $R_{b/t} \rightarrow 1$, the concentrations at the bottom and on the top of the screen tend to be equal, meaning that the tracer concentration tends to be homogenous in the screened interval. In ideal cases (if the recirculation flow rate is sufficient to ensure the perfect homogenization of the tracer), $R_{b/t}$ should reach 1. Conversely, the ratio $R_{b/t}$ decreases when significant differences in concentrations are observed between the bottom and the top of the tested interval. Thus, lower ratio values can be associated to non-perfect mixing conditions, meaning that the tracer distribution is non uniform along the tested interval. In practice, this means that a significant portion of the tracer mass would be preferentially carried out of the well and lost before reaching the mixing pump located in the bottom of the well.

The ratio $R_{b/t}$ is thus defined as the ratio between the value of the tracer concentration stabilization at the bottom of the tested interval and the value of the tracer concentration stabilization at the top and can be calculated using:

$$R_{b/t} = \frac{C_{w,stab,Nz}}{C_{w,stab,Nz-Nz_{scr}+1}} = \prod_{i=Nz-Nz_{scr}+2}^{Nz} \frac{Q_{inj} - (i-1)\frac{Q_{inj}}{Nz_{scr}} + Q_{recirc}}{\frac{Q_t^{in}}{Nz_{scr}} + Q_{inj} - (i-1)\frac{Q_{inj}}{Nz_{scr}} + Q_{recirc}} \quad (9)$$

Note that the mathematical developments used to calculate the ration $R_{b/t}$ (Eq. 9) are provided in Appendix B.

2.1.5. The inverse approach

Besides simulating tracer concentration profiles depending on flow and experimental conditions, the purpose of developing a discrete model is to be able to interpret field data and estimate groundwater fluxes for both perfect and non-perfect mixing conditions. To do so, the discrete model is coded in MATLAB® and an inverse approach is used to estimate the optimal value of groundwater flow accounting for tracer concentration evolutions measured in the field. Note that the tracer concentration is measured within the recirculation loop (Fig 1)

and the associated tracer evolution stands for the tracer evolution at the bottom the tested interval (to the level of the pump).

First, the tested interval is discretized into i elements of size Δz depending on the geometry of the tested well and the time is discretized into Nt time steps Δt. Δz and Δt are chosen so the Courant Number (Eq. 8) does not exceed 1. Then, Equations 1, 2, 3 and 4 are used to model the tracer concentration evolution along the water column. Calculations are made over a large range of groundwater flow rates. For each value of groundwater flow rates tested, the RMSE (Root-Mean-Square Error) between the concentration evolution modelled in the bottom of the well (i = Nz) using the discrete model and the tracer concentration measured in the field is calculated. Then, the nonlinear optimization function *fminsearch*, based on the Nelder-Mead simplex algorithm (Lagarias et al., 1998), automatically determines the value of groundwater flow rate associated with the minimal value of RMSE, which allows estimating the optimal value of groundwater flow accounting for the measured tracer concentration evolution. In complement, the same approach can be used to interpret the field data using the classical model (Brouyère et al., 2008) in order to validate the inverse approach applied here and to compare both models.

2.2. Field application

The adequacy and relevance of the new FVPDM discrete model was tested and illustrated using the field measurements presented by Jamin and Brouyère (2018). The aim of this study was to monitor transient groundwater fluxes in the alluvial aquifer of the River Meuse near Liège (Belgium), where subsurface is characterized by an important vertical heterogeneity related to the presence of different layers of alluvial deposits inducing variable hydraulic properties with depth (see Wildemeersch et al. (2014) for more details). In their study, Jamin and Brouyère (2018) observed that the mixing flow rate applied during the experiment was too low compared to the groundwater transit flow rate, which affected the groundwater flow estimate. We propose here to test this assumption by reinterpreting their measurements with the discrete model and to compare the associated results (groundwater fluxes estimates) with the one obtained using the classical approach.

2.2.1. Description of FVPDM tests

Jamin and Brouyère (2018) performed two FVPDM tests simultaneously in a single borehole (Pz19), equipped with two internal piezometers. The first piezometer (Pz19_shallow) is screened over 0.9 m-length in the upper part of the aquifer (at 4.1 m-depth) constituted of fine

sandy gravels. The second piezometer (Pz19_deep) is screened over 1.8 m-length in the lower part of the aquifer (at 7.95 m-depth) consisting of coarser gravels and pebbles. Previous studies showed that the mean hydraulic conductivity for the alluvial aquifer varies between $2x10^{-3}$ and $1.2x10^{-1}$ $m.s^{-1}$ and that the hydraulic conductivity is higher in the lower part of the aquifer than in the upper part (Brouyère, 2001; Wildemeersch et al., 2014).

Transient flow conditions were imposed by pumping groundwater at different rates for more than 36 hours in a pumping well located at 5 m from Pz19. The pumping rate schema applied over time at the pumping well, including phases with no pumping to approach ambient groundwater flow conditions, is detailed in Figure 3a. Table 1 presents experiment parameters for each FVPDM test.

Jamin and Brouyère (2018) applied the classical approach developed by Brouyère et al. (2008), assuming the perfect homogenization of the tracer, to interpret the tracer concentration evolution measured in the bottom of each piezometer during the tracer injection. Concerning the FVPDM conducted in Pz19_shallow, a linear evolution of the measured groundwater flux with the pumping rate has been found, which is logical and consistent (the higher the pumping rate, the higher the flux). However, for the FVPDM conducted in Pz19_deep, this linear relationship was not observed, which was surprising. To explain this, the authors made the assumption that the mixing flow rate applied during the experiment conducted in Pz19_deep could have been too low compared to the groundwater transit flow rate passing through the well screen. Indeed, for Pz19_shallow (linear relation), the maximum groundwater transit flow rate was estimated to be $5.26x10^{-6}$ $m^3.s^{-1}$, while for Pz19_deep the maximum groundwater transit flow rate was estimated 70 times higher ($3.80x10^{-4}$ $m^3.s^{-1}$). In both cases, the recirculation flow rate applied was $Q_{recirc} = 1.9x10^{-4}$ $m^3.s^{-1}$, which means that for Pz19_deep the recirculation flow rate was much lower than the transit flow rate estimated. Thus, a significant portion of the tracer mass is suspected to be preferentially carried out of the well and lost before reaching the mixing pump located in the bottom of the well, meaning that the flow estimated in Pz19_deep could be overestimated.

Table 1Details about the experiment are available in Jamin and Brouyère (2018)

	Pz19_shallow	**Pz19_deep**
Depth of the screen [m]	4.1	7.95
Screen length e_{scr} [m]	0.9	1.8
Inner radius of the well r_w [m]	0.0254	

Height of the water column h_w [m]	2.05	6.93
Water volume in the well V_w [m^3]	$4.9x10^{-3}$	$1.53x10^{-2}$
Tracer	Sulforhodamine B	Uranine
Injection rate Q_{inj} [$m^3.s^{-1}$]	$5.71x10^{-7}$	$3.23x10^{-6}$
Tracer concentration in the injection water C_{inj} [ppb]	500	250
Recirculation rate Q_{recirc} [$m^3.s^{-1}$]	$1.9x10^{-4}$	

2.2.2. Application of the new discrete model and objectives

We propose here to test the effect of the non-perfect mixing on FVPDM results by reinterpreting the field measurements with the discrete model and to compare the associated results (groundwater fluxes estimates) with the one obtained using the classical solution. Firstly, for Pz19_shallow, results of Jamin and Brouyère (2018) suggested a perfect homogenization of the tracer along the tested interval. Therefore, groundwater fluxes estimates with the new discrete model obtained here are expected to be similar to the one obtained with the classical approach as proposed in Jamin and Brouyère (2018). Studying this "perfect mixing" should allow validating the use of the discrete model as well as the associated inverse approach that allows finding the optimal value of groundwater flow accounting for the measured tracer concentration evolution. Secondly, the assumption of non-perfect mixing will be tested using the discrete model by simulating concentration profiles within the tested interval for Pz19_deep. By comparing groundwater fluxes estimates obtained with both the classical and the new discrete model, we aim to assess the effect of the recirculation rate on tracer distribution within the well.

Parameters used to implement the discrete model are similar as the one used in Jamin and Brouyère (2018) (Table 1). For Pz19_shallow, h_w was discretized in 64 elementary cells (Δz = 0.032 m) with 29 cells in the screened interval. For Pz19_deep, h_w was discretized in 125 elementary cells (Δz = 0.055 m) with 33 cells in the screened interval. For both cases, Δt was fixed at 0.1 sec. Thus, Courant numbers were respectively 0.03 and 0.05 for Pz19_shallow and Pz19_deep, ensuring the stability of computations. The inverse approach previously described was applied to estimate groundwater fluxes from tracer concentration evolutions for both the new discrete FVPDM model and the classical model.

2.3. Sensitivity analysis

In order to generalize the results obtained with the discrete model, a sensitivity analysis was performed to assess the effect of recirculation flow rate and of injection flow rate on results of

FVPDM tests. This aims to define limits of the method, advantages of the discrete model and to address recommendations about the use of FVPDM in different flow conditions.

Just as proposed by Brouyère et al. (2005, 2008), sensitivity analysis was made using nondimensional variables for the sake of generality. To do so, concentration terms were normalized according to the concentration in the tracer fluid C_{inj}, while flow rate terms were normalized according to the critical injection rate Q_{cr}. As a reminder, Q_{cr} corresponds to the injection rate above which the transit flow rate Q_t is cancelled (radially diverging flow prevails), making the flow estimation impossible. Thus, normalized tracer concentration in the well is $C_w^* = C_w/C_{inj}$ and normalized injection and recirculation rates are respectively $Q_{inj}^* = Q_{inj}/Q_{cr}$ and $Q_{recirc}^* = Q_{recirc}/Q_{cr}$.

In the classical approach, Brouyère et al. (2005) proposed to normalize time t using T_w, corresponding to the time needed to replace water in the tested interval (V_w) at the critical injection rate (Q_{cr}). Such approach requires assuming an instantaneous mixing of the tracer within the tested interval, which is not applicable for the discrete model in which recirculation flow rate is considered and tracer repartition within the well modelled. In this case, normalizing time requires considering the solute transport in depth depending on Q_{inj} and Q_{recirc}, which can be expressed using a lag time parameter $\tau_i = \frac{z_i \pi r_w^2}{Q_{inj} + Q_{recirc}}$, corresponding to the time required for the tracer to reach depth z_i. Therefore, time was normalized such as $t_i^* = {t - \tau_i}/{T_{wi}}$, where T_{wi} corresponds to the time needed to replace the water in each cell at the critical injection rate ($T_{wi}=V_{wi}/Q_{cr,i}$).

3. Results

3.1. Field application

3.1.1. Reproduction of field data

Figure 3 presents the interpretation of the FVPDM tests performed by Jamin and Brouyère (2018) in the alluvial aquifer of the River Meuse. These results correspond to optimal values of groundwater fluxes estimated using the inverse approach either with the classical model or the discrete model.

Figures 3b, c and d focus on the experiment conducted in the piezometer Pz19_shallow. Field data are very well reproduced with both models for all steps of pumping rates applied

(Figure 3b). Likewise, groundwater fluxes estimates are very similar with both models (Figure 3c-d) and the linear relationship between pumping rate and groundwater fluxes is verified with both models (Fig. 3d) and the consistency and similarity of results obtained with both models allow validating the discrete model.

Figures 3e, f and g focus on the experiment conducted in the piezometer Pz19_deep. Figures 3e compares the tracer concentration evolution measured in the bottom of the well during the experiment (blue line) with modelled tracer concentration evolutions (the yellow line being associated to the classical approach and the green line to the discrete model). Once again, field data can be very well reproduced with both models, with RMSEs between field data and modelled data of 0.29 ppb for both cases. However, contrary to results obtained for Pz19_shallow, groundwater fluxes estimated with the classical model are significantly different and systematically higher than groundwater fluxes estimated with the discrete model (Figure 3f). Using the classical approach, apparent Darcy fluxes are estimated between 5.98×10^{-4} and 4.5×10^{-3} $m.s^{-1}$ (Q_t between 5.47×10^{-5} and 4.11×10^{-4} $m^3.s^{-1}$) whereas the discrete model estimates apparent Darcy fluxes between 5.28×10^{-4} and 2.39×10^{-3} $m.s^{-1}$ (Q_t between 4.83×10^{-5} and 2.19×10^{-4} $m^3.s^{-1}$). Interestingly, the higher the pumping rate (and groundwater fluxes), the higher the difference on the fluxes estimates. When pumping at 50 $m^3.h^{-1}$, difference on fluxes estimates reaches 81.6 %. However, the difference still remains important for lower fluxes since under ambient groundwater flow conditions (phases with no pumping), the difference on estimated fluxes is 24 %.

Figure 3g shows groundwater fluxes evolution with pumping obtained with each model. While the classical model predicts an exponential relationship between calculated groundwater fluxes and pumping rates (in accordance with results of Jamin and Brouyère (2018)), the discrete model predicts a linear relationship between both. Results suggest that each 10 $m^3.h^{-1}$ increment at the pumping well corresponds to an increment of 3.06×10^{-4} $m.s^{-1}$ (i.e. 26.5 $m.d^{-1}$) in the apparent groundwater flux measured in Pz19_deep (in Pz19_shallow each 10 $m^3.h^{-1}$ increment at the pumping well is associated to an increment of 1.77×10^{-5} $m.s^{-1}$ (i.e. 1.5 $m.d^{-1}$) in the apparent groundwater flux).

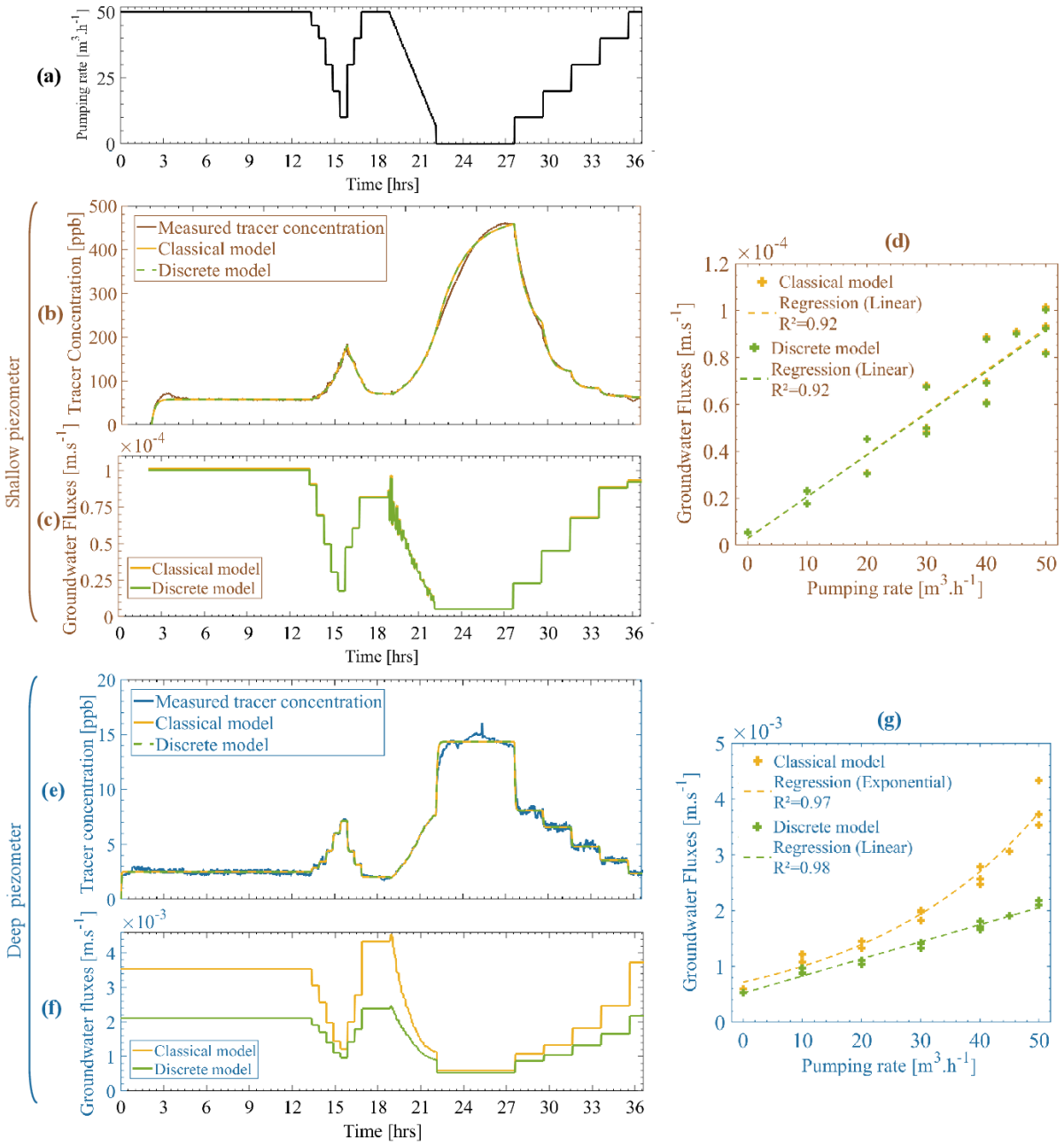

Figure 3. a) Pumping rates applied during the experiment in the pumping well located near the piezometer Pz19. Figures b, c and d focus on the interpretation of the FVPDM test performed in Pz19_shallow using either the classical model (yellow curves) or the discrete model (green curves). Figure b presents tracer concentration evolutions measured (brown line) and modelled. Figure c present associated groundwater fluxes estimates with both models. Figure d presents the evolution between pumping rate and groundwater fluxes. Likewise, figures e, f and g focus on the interpretation of the FVPDM test performed in Pz19_deep.

3.1.2. Simulation of tracer concentration profiles

In order to better understand why the classical model can not be applied for the deeper piezometers, the tracer concentration profiles at the end of the first stage of pumping are simulated using the discrete model (Figures 4a and 4c). For both piezometers, the shapes of concentration profiles with depth are similar, with uniform concentrations in the tube and a

concentration decrease with depth in the screened interval. However, the ratio $R_{b/t}$ (between the concentration at the bottom and the concentration at top of the screen) is 0.98 for the shallow piezometer (Figure 4a) while 0.37 for the deep piezometer (Figure 4c). This means that the tracer gradient is 2.6 times more important in the deep piezometer than in the shallow one.

Thus, for Pz19_shallow, even if the tracer concentration is not strictly homogeneous in the screened interval, the concentration difference between the top and the bottom of this interval is relatively low. Therefore, tracer concentration evolutions are relatively similar all along the screen and both models (discrete and classical) predict similar tracer concentration evolutions over time (Figure 4c). Conversely, for Pz19_deep, a significant difference of concentrations is observed between the top and the bottom of the screen (blue lines, Figure 4d). If the classical model is used in this case, the tracer concentration measured at the bottom of the interval is reproduced (yellow line), which necessarily requires to consider a higher value of groundwater flow. That is why, in the case of non-perfect mixing conditions, the classical approach leads to overestimate the effective value of groundwater fluxes.

In addition, both models show significant differences concerning tracer concentration evolutions before tracer concentration stabilizes (transient stage). A significant time lag is observed between the injection start and the start of concentration rise with the discrete model (while the concentration instantaneously starts increasing with the classical approach). Then, with the discrete model, the tracer concentration increases stepwise. Blue lines show oscillations (sequential plateaus) at the beginning of the experiment due to the water reinjection on top of the well and to the non-instantaneous homogenization of the tracer within the well.

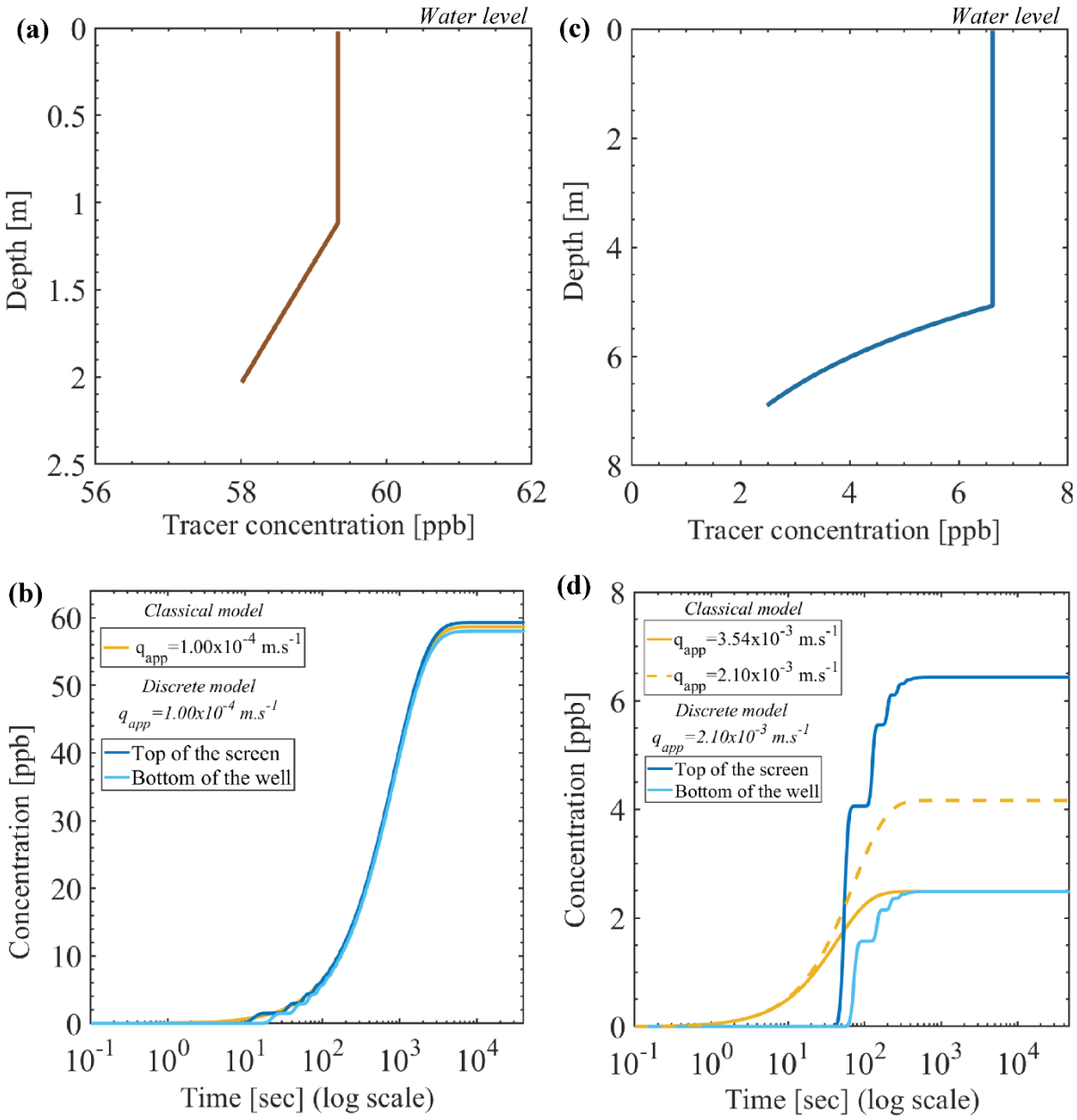

Figure 4. a) Tracer concentration profiles modelled for t = 13.28 hours for Pz19_shallow using the discrete model considered the optimal value of groundwater fluxes estimated (1.00x10^{-4} m.s^{-1}). b) Tracer concentration evolution over time modelled in Pz19_shallow for the first stage of pumping considering the optimal value of groundwater fluxes (1.00x10^{-4} m.s^{-1}) obtained with both models. c) Tracer concentration profiles modelled for Pz19_deep using the discrete model considered the optimal value of groundwater fluxes estimated (2.10x10^{-3} m.s^{-1}). b) Tracer concentration evolution over time modelled in Pz19_deep for the first stage of pumping considering optimal values of groundwater fluxes (3.54x10^{-3} m.s^{-1} for the classical model - solid yellow line - and 2.10x10^{-3} m.s^{-1} for the discrete model - blue lines). The dotted yellow line corresponds to the tracer concentration evolution modelled with the classical model by considering the optimal value of groundwater fluxes estimated with the discrete model (2.10x10^{-3} m.s^{-1}).

3.2. Sensitivity analysis

3.2.1. Non-perfect mixing domain

Figure 5a shows the value of the ratio $R_{b/t}$ (ratio between the stabilized tracer concentration at the bottom of the tested interval and the stabilized tracer concentration on the top of the tested interval) depending on Q^*_{recirc} and Q^*_{inj}. This allows evaluating if concentrations are uniform along the screened interval according to flow conditions. This plot is established using Equation 9 and nondimensional variables, so results are independent of the screened interval length. Figure 5b shows the difference between fluxes estimated using the classical model and fluxes estimates using the discrete model depending on flow and experimental conditions. To obtain this plot, concentrations profiles were first simulated for different values of Q^*_{recirc} and Q^*_{inj} using the discrete model. Then, concentrations evolutions modelled at the bottom of the screened interval are interpreted using the classical model. Associated estimated values of groundwater fluxes are compared with effective values of groundwater fluxes. This approach aims to define in which conditions the classical model is well suited to interpret field measurements.

As underlined in Figure 5, results can be divided into two domains depending on the value of Q^*_{recirc}. First, for large values of Q^*_{recirc} (> 5), the difference of concentrations within the screened interval is < 5% (Figure 5a), meaning that the concentration can be considered uniform in the tested interval. Therefore, data interpretation is similar regardless of the model applied (discrete or classical), with differences on groundwater fluxes estimates < 3.5 % (Figure 5b). In this case, results are similar for any value of Q^*_{inj}. Conversely, for lower values of Q^*_{recirc} (< 5), concentrations can not be considered uniform along the tested interval and the lower the value of Q^*_{recirc} the more important the gradient of the concentration with depth (Figure 5a). Therefore, the use of the classical model (that only considers perfect mixing and homogenization of the tracer) to interpret field measurements can induce significant discrepancies on groundwater fluxes estimates (Figure 5b). The classical approach systematically overestimates groundwater fluxes with errors > 50 % as soon as Q^*_{recirc} < 0.5 and errors 100% for Q^*_{recirc} < 0.3 (meaning that the estimated fluxes are at least twice more important than effective fluxes). Besides, results show that, for low values of Q^*_{recirc}, the value of Q^*_{inj} has also significant effects on tracer distribution and thus on groundwater fluxes estimates. Thus, errors on fluxes estimates are higher for lower values of Q^*_{inj}.

Figure 5a also allows defining the limit of the FVPDM method. Indeed, the limit of the method is reached as soon as the ratio $R_{b/t}$ reaches 0, which means that the tracer never reaches the bottom of the well (at least at a concentration which is below detection limit) and data interpretation becomes impossible. This limit is reached when Q^*_{recirc} < 0.04 for Q^*_{inj}= 0.01 or when Q^*_{recirc} < 0.02 for Q^*_{inj}= 0.05. Note that when Q^*_{inj}= 0.1, this limit is never reached, meaning that the tracer systematically reaches the bottom of the screen. In this case, the injection flow rate is necessarily high enough to allow the tracer to reach the bottom, even a small portion.

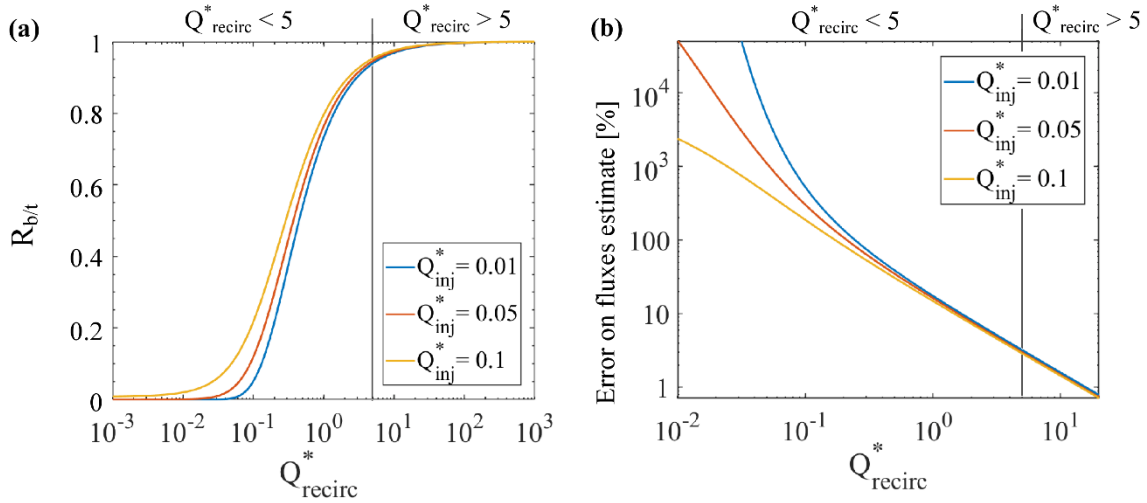

Figure 5. a) Value of the ratio $R_{b/t}$ depending on Q^*_{recirc} and Q^*_{inj} ($Q^*_{recirc} = Q_{recirc}/Q_{cr}$; $Q^*_{inj} = Q_{inj}/Q_{cr}$) b) Difference between fluxes estimated using the classical model and fluxes estimates using the discrete model depending Q^*_{recirc} and Q^*_{inj}. For both plots, the vertical line demarcates the perfect mixing domain (Q^*_{recirc}>5) from the non-perfect mixing domain (Q^*_{recirc}<5).

3.2.2. Tracer homogenization within the wellbore

Figure 6 shows the effect of the recirculation rate on tracer concentration evolutions at different depths. In complement to Figure 5, it allows visualizing the effect of Q^*_{recirc} and Q^*_{inj} on concentration profiles. It clearly confirms that the higher the value of Q^*_{recirc}, the better the tracer homogenization within the well. Thus, for Q^*_{recirc}= 20 tracer concentration evolutions are very similar regardless the depth considered with a ratio $R_{b/t}$of 0.985 and 0.988 for Q^*_{inj} = 0.03 and 0.1 respectively (Fig 6c and f). For lower values of Q^*_{recirc}, the tracer concentration gradient in the well is way more important. For instance, the ratio $R_{b/t}$ reaches 0.261 for $Q^*_{recirc} = 0.2$ and Q^*_{inj} = 0.03 and significant differences in tracer concentration evolutions are observed within the tested interval (Fig 6a). Note that the ratio $R_{b/t}$ is systematically higher for

451 Q^*_{inj} = 0.03 than for Q^*_{inj} = 0.1, in agreement with results presented in Figure 5a. This means
452 that higher injection rates contribute to better mixing within the tested interval.

453 Figure 6 also shows that results obtained with both approaches are similar for large
454 values of Q^*_{recirc}. For lower values of Q^*_{recirc}(Fig 6a, b, d and e), the classical approach does
455 not reflect the tracer concentration distribution but describes the average concentration. Indeed,
456 the stabilized concentration obtained with the classical model corresponds to the mean of
457 stabilized concentrations obtained along the screened interval with the discrete approach.

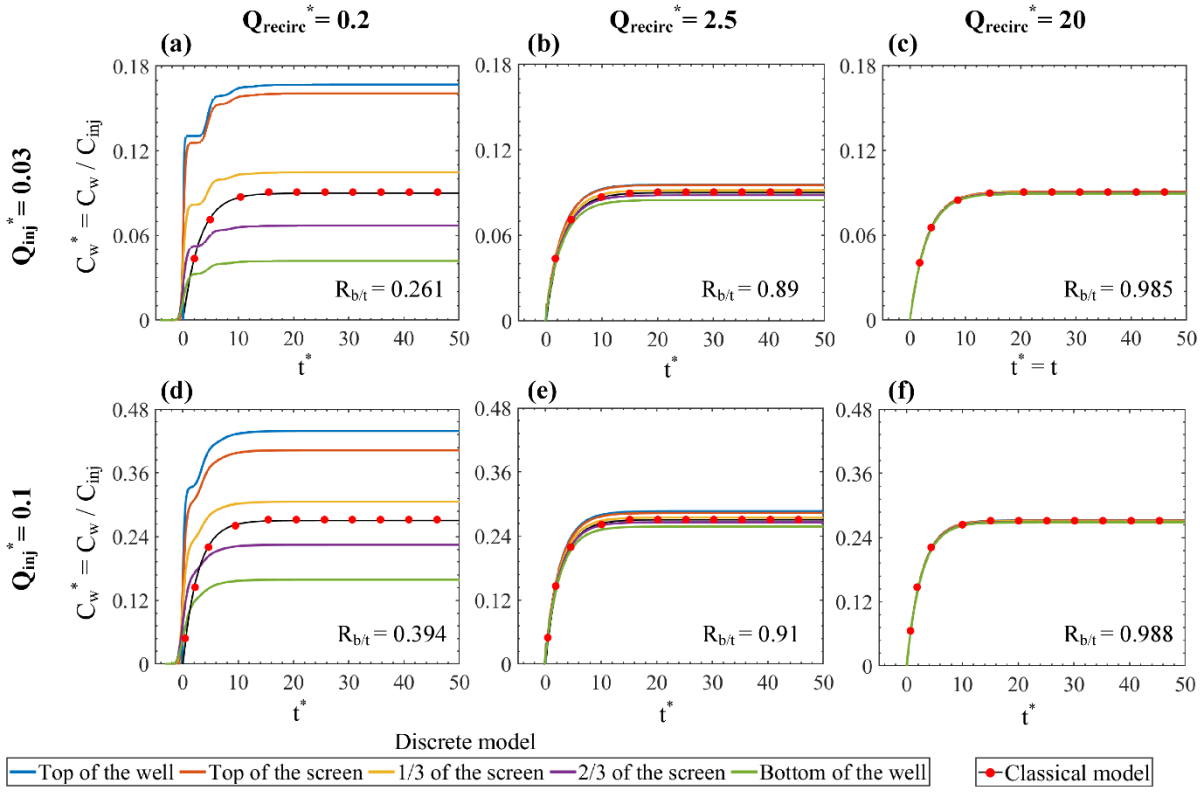

458

459 **Figure 6. Effect of Q^*_{recirc} and Q^*_{inj} on tracer concentration evolutions observed at different depths of the**
460 **screened interval. Figures a, b and c are associated to Q^*_{inj} = 0.03 and to values of Q^*_{recirc} equals to 0.2, 2.5**
461 **and 20 respectively. Figures d, e and f present results for Q^*_{inj} = 0.1.**

462 ## 4. Discussions

463 Results show that mixing within the tested interval depends on the recirculation flow rate
464 compared to the groundwater flow rate crossing the well screens (Q^*_{recirc}). When Q^*_{recirc} > 5,
465 the recirculation flow can be considered high enough compared to groundwater fluxes to ensure
466 the homogenization of the tracer within the tested interval. In this case of perfect-mixing
467 conditions, the concentration evolution measured in the bottom of the well can be interpreted
468 either with the classical model developed by Brouyère et al. (2008) or with the discrete model
469 presented here. Groundwater fluxes estimates will be similar with both models (with differences

on estimates less than 5%). This was experimentally validated through FVPDM tests performed in the alluvial aquifer of the River Meuse. For the shallow piezometer (Pz19_shallow), data interpretation (with both models) led to estimate Q_{cr} varying between 1.44×10^{-5} and 7.79×10^{-7} $m^3.s^{-1}$ meaning that the values of Q^*_{recirc} during the experiment varied between 13.2 and 244. Note that, since the classical model is easier to implement, its use should be preferred in case of perfect-mixing conditions.

Conversely, for non-perfect mixing conditions ($Q^*_{recirc} < 5$), results demonstrate the importance of using the discrete FVPDM model introduced in this paper to interpret concentration evolution curves. Indeed, the classical model may lead to high overestimates of groundwater fluxes, as demonstrated with the interpretation of data collected in piezometer Pz19_deep. In this case, the value of Q^*_{recirc} varies between 0.27 and 1.25 during the experiment. Such values suggest the recirculation flow rate is not high enough to ensure the homogenization of the tracer within the tested interval. It leads to large errors on fluxes estimates while using the classical model (between 14 and 82 %), in accordance with results presented in Figure 5b. Whereas the classical model is only applicable when $Q^*_{recirc} > 5$, the discrete model allows estimating fluxes even if experimental conditions are not ideal ($Q^*_{recirc} < 5$). In piezometer PZ19_deep for instance, considering the groundwater fluxes reached (2.26×10^{-4} $m^3.s^{-1}$) when pumping at 50 $m^3.h^{-1}$, the recirculation flow rate should have been around 128 $L.min^{-1}$ (against 11.4 $L.min^{-1}$) to ensure the homogenization of the tracer and to make possible the use of the classical model, which is hardly feasible in practice.

Concerning the measurements made in piezometer PZ19_deep, groundwater flow estimates remain relatively high, compared to the one obtained in piezometer PZ19_shallow. These results are in good agreement with the fact that higher values of hydraulic conductivities are found in the lower part of the aquifer (Wildemeersch et al., 2014). However, in case of very high groundwater flow, non-laminar flow could occur. Since, the Darcy's law is not applicable for non-laminar flow (Fourar et al., 2004; Quinn et al., 2011), this could explain why a non-linear relationship has been initially found between the groundwater flux and the pumping rate. However, by considering the maximal groundwater flux estimated with the discrete model, it can be assumed that the flow is laminar if the mean pore size diameter of the porous media is lower than 5 mm. In this case, the Reynolds number is lower than 10, which ensures laminar flow (Bear, 1972). The mean pore size diameter of the porous media has never been measured in the field but the lower part of aquifer consists of coarse gravels filled with sand and silt.

Knowing that, it is consistent to assume that the mean pore size diameter is lower than 5 mm. Moreover, the fact that a linear relationship between the groundwater flux and the pumping rate with the improved model tends to confirm that laminar flow effectively occurs.

Likewise, the discrete model also allows modelling the time lag that can exists between the injection start and the concentration rise. This time lag is not simulated with the classical approach since the mixing is assumed to be instantaneous in the tested interval. For the classical model, the time required to reach 99% of the stabilized concentration is estimated to be $-\frac{V_w}{Q_{inj}+Q_t^{in}}\ln 0.01$, which implies the concentration stabilization is reached simultaneously everywhere within the tested interval. In case of non-perfect mixing conditions, the time required to reach 99% of the stabilized concentration is estimated to be $-\frac{V_{wi}}{Q_{inj,i}+Q_{t,i}^{in}+Q_{recirc}}\ln 0.01$ (from Equation A-9). This involves that the time required to reach the steady-state increases with depth, which is perfectly consistent, and that the higher the recirculation flow rate, the shorter the stabilization time.

Lastly, this study also allows discussing the limits of FVPDM to investigate groundwater fluxes. Thus, although the discrete model allows interpreting FVPDM tests while experimental conditions are not ideal (Q_{recirc}^{*} < 5), the limit of the method is reached for very low values of Q_{recirc}^{*} (< 0.4 for Q_{inj}^{*} = 0.01 or < 0.01 for Q_{inj}^{*} = 0.05). In this case, the recirculation flow rate is so weak compared to the groundwater flow rate that the tracer completely dissipates in the tested interval and the measured concentration at its bottom is zero (Figure 5).

5. Conclusion

The discrete FVPDM model introduced in this paper allows assessing the vertical transport of the tracer along the well axis by explicitly considering the recirculation flow rate in the interpretation of FVPDM tests. This study shows that, when performing FVPDM in the field, it is essential to accurately consider the value of the recirculation flow rate compared to the groundwater flow rate crossing the well screens. Neglecting the recirculation flow rate during field data interpretation can lead to significant overestimates of groundwater fluxes. While the perfect repartition of the tracer is classically assumed when interpreting FVPDM, it can be technically difficult to apply and maintain a mixing flow rate higher than groundwater transit flow rate without significantly perturbating the flow pattern around and within the tested well. The discrete model introduced here allows interpreting FVPDM conducted in

non-perfect mixing conditions and thus increases the range of fluxes that can be investigated with FVPDM tests.

Non-perfect mixing conditions can be encountered in very permeable aquifer materials, as highlighted in this paper, but also when tests are performed in long-screened wells. Moreover, the discrete model can also be used to simulate vertical variations of groundwater flow or preferential horizontal flow paths, since the groundwater flow value is set for each cell of the domain. Therefore, the discrete model offers new perspectives for the characterization of groundwater flow, including the possibility of investigating heterogeneous and fractures aquifers.

Funding sources

Nataline Simon is a beneficiary of the IPD-STEAM fellowship supported by the Special Funds for Research. This work is supported by the FNRS Belgium [grant no. J.0023.22]

Appendix A

The domain (the volume of water) is discretized into i elementary cells with vertical size Δz_i (i=1, 2, …, Nz) as shown in Figure 2a. Mass balance equations are written for each elementary cell considering that the mass of tracer M_i, diluted into each volume of water V_{wi}, changes over time depending on flow rates entering ($\sum Q_{entering,i}$) and leaving the cell i ($\sum Q_{leaving,i}$) and their respective concentrations in tracer $C_{entering,i}$ and $C_{leaving,i}$:

$$\frac{dM_i}{dt} = V_{wi}\,\frac{dC_{w,i}}{dt} = \sum Q_{entering,i}\,C_{entering,i} - \sum Q_{leaving,i}\,C_{leaving,i} \qquad \text{(A-1)}$$

Note that mass balance equations are written assuming that density effects, that could be induced by the presence of the tracer in the water, are negligible. Indeed, density effects can be neglected if density changes compared to the density of the water are lower than 2% (Dassargues, 2018). This condition is verified if the tracer injected during FVPDM tests has a concentration lower than 2000 ppb.

In the tube interval for i=1:Nz-Nz_{scr} (Figure 2a, b and c), only vertical flow circulation occurs, meaning that flow rate terms accounting for water and solute transport within the

tubewell are the injection flow rate Q_{inj} and the recirculation flow rate Q_{recirc} (ensured by the mixing pump in the bottom of the tested interval).

The tracer injection point takes place at top of the well (i = 1). Flow entering the cell includes the recirculation flow rate Q_{recirc} and the injection flow rate Q_{inj} and tracer concentrations associated with these flow rates are $C_{w,Nz}^{j-1}$ and C_{inj} respectively (Figure 2b). C_{inj} corresponds to the tracer concentration in the injection water (tracer tank in Figure 1) and $C_{w,Nz}^{j-1}$ corresponds to the tracer concentration in the water pumped in the bottom of the well (i = Nz) at j-1 and reinjected in its top at j. The tracer concentration reinjected at j=1 is C_0, corresponding to the initial tracer concentration in groundwater and within the well at initial time. Thus, the mass balance equation applied for i = 1 and j > 2 (Figure 2b) is given by:

$$V_{wi}\ \frac{dC_{w,i}}{dt} = \left[Q_{recirc}\ C_{w,Nz}^{j-1} - Q_{recirc}\ C_{\mathrm{w},1}^{j} + \ Q_{inj}C_{inj} - Q_{inj}C_{\mathrm{w},1}^{j}\right] \qquad \text{(A-2)}$$

Likewise, the mass balance equation is written for each cell within the tube interval for i > 2 (Figure 2c) following:

$$V_{wi}\ \frac{dC_{w,i}}{dt} = \left[Q_{recirc}\ C_{\mathrm{w},i-1}^{j} - Q_{recirc}\ C_{\mathrm{w,i}}^{j} + \ Q_{inj}C_{\mathrm{w},i-1}^{j} - Q_{inj}C_{\mathrm{w,i}}^{j}\right] \qquad \text{(A-3)}$$

For each cell i, the tracer concentration calculated for i-1 ($C_{\mathrm{w},i-1}^{j}$) is used to set the tracer concentration entering in the volume V_{wi} and associated with both the recirculation flow rate Q_{recirc} and the injection flow rate Q_{inj}.

In the screened interval (Figures 2a, d and e), besides the recirculation flow rate, flow rate terms include exchanges between the well and the test aquifer system (transit flow rate). Thus, the transit flow rate $Q_{t,i}^{in}$ corresponding to the flow crossing the well under injection conditions for each interval i is included in the mass balance equations. The injection flow rate is distributed along the screen and a portion $Q_{inj,i}$ of the total injection flow rate (Q_{inj}) leaves the screen at each cell.

Considering this, the mass balance equation is established for the screened interval for i = Nz - Nz_{scr} + 2 : Nz (Figures 2e) following:

$$\begin{aligned} V_{wi}\ \frac{dC_{w,i}}{dt} = \big[&Q_{recirc}\ C_{\mathrm{w},i-1}^{j} - Q_{recirc}\ C_{\mathrm{w},i}^{j} + Q_{t,i}^{in}\ C_0 - Q_{t,i}^{in}\ C_{\mathrm{w},i}^{j} \\ &+\ Q_{inj,\,i-1}\ C_{\mathrm{w},i-1}^{j} - Q_{inj,i}\ C_{\mathrm{w,i}}^{j} - (Q_{inj,i-1} - Q_{inj,i})C_{\mathrm{w},i}^{j}\big] \end{aligned} \qquad \text{(A-4)}$$

584 And for i = Nz-Nz_{scr} + 1 (Figures 2d , screen top) following:

$$V_{wi}\frac{dC_{w,i}}{dt} = \left[Q_{recirc}\,C^{j}_{\mathrm{w},i-1} - Q_{recirc}C^{j}_{\mathrm{w,i}} + Q^{in}_{t\ ,i}C_0 - Q^{in}_{t\ ,i}C^{j}_{\mathrm{w,i}} + Q_{inj}C^{j}_{\mathrm{w},i-1} - Q_{inj,i}C^{j}_{\mathrm{w,i}} - (Q_{inj} - Q_{inj,i})C^{j}_{\mathrm{w,i}}\right] \quad \text{(A-5)}$$

585

586 Mass balance equations previously defined (Eq. A-2, A-3, A-4 and A-5) can be numerically
587 evaluated through the forward difference expression approximant of Δt:

$$\frac{dC_{w,i}}{dt} \approx \frac{C_{w,i}\,(t+\Delta t) - C_{w,i}\,(t)}{\Delta t} = \frac{C^{j+1}_{w,i} - C^{j}_{w,i}}{\Delta t} \quad \text{(A-6)}$$

588 Thus, the concentration of tracer C_w can be calculated for each cell and each time step $C^{j}_{w,i}$.The
589 initial conditions are $C^{1}_{w,i}$ = C_0 (the tracer concentration at j = 1 corresponds to the tracer
590 concentration in the aquifer and in the well at initial time, before tracer injection).

591 **Appendix B**

592 To calculate the ratio $R_{b/t}$, it is possible to analytically solve the first order linear differential
593 Equation A-4 (the mass balance equation applied along the screen). By considering the initial
594 condition $C_{w,i}$ ($t = t_0$) = C_0, the concentration evolution can thus be expressed for each cell i
595 located in in the screened interval as:

$$C_{w,i}(t) = \frac{C_{w,i-1}(Q_{inj,i-1} + Q_{recirc}) + \left(C_0(Q_{out,\,i} + Q_{recirc}) - C_{w,i-1}(Q_{inj,i-1} + Q_{recirc})\right)e^{-\frac{(Q_{out,\,i}+Q_{recirc})}{V_{wi}}(t-t_0)}}{(Q_{out,\,i} + Q_{recirc})} \quad \text{(A-7)}$$

596 Where

$$Q_{out,\,i} = Q^{in}_{t,i} + Q_{inj,\,i-1} \quad \text{(A-8)}$$

597

598 Considering C_0 = 0 (tracer concentration in the aquifer and within the well at initial time is
599 negligible), Equation A-7 becomes:

$$C_{w,i}(t) = \frac{C_{w,i-1}(Q_{inj,i-1} + Q_{recirc})\left(1 - e^{-\frac{(Q_{out,\,i}+Q_{recirc})}{V_{wi}}(t-t_0)}\right)}{(Q_{out,\,i} + Q_{recirc})} \quad \text{(A-9)}$$

600 Using Equation A-9, the stabilized concentration expected for t→ ∞ for each cell i can be
601 expressed as:

$$C_{w,stab,i} = \lim_{t \to \infty} \frac{C_{w,i-1}(Q_{inj,i-1} + Q_{recirc}) + \left(1 - e^{-\frac{(Q_{out,i} + Q_{recirc})}{V_{wi}}(t-t_0)}\right)}{(Q_{out,i} + Q_{recirc})} = \frac{C_{w,stab,i-1}(Q_{inj,i-1} + Q_{recirc})}{(Q_{out,i} + Q_{recirc})} \quad \text{(A-10)}$$

In the case of homogeneous flow conditions along the screen, $Q_{inj,i-1}$ can be expressed as:

$$Q_{inj,i-1} = Q_{inj} - (i-1)\frac{Q_{inj}}{Nz_{scr}} \quad \text{(A-11)}$$

Meaning that:

$$Q_{out,i} = \frac{Q_t^{in}}{Nz_{scr}} + Q_{inj} - (i-1)\frac{Q_{inj}}{Nz_{scr}} \quad \text{(A-12)}$$

Following Equations A-10, A-11 and A-12, the ratio between the stabilized tracer concentration for cell i and the stabilized tracer concentration for cell i-1 is given for homogeneous flow conditions by:

$$\frac{C_{w,stab,i}}{C_{w,stab,i-1}} = \frac{Q_{inj,i-1} + Q_{recirc}}{Q_{out,i} + Q_{recirc}} = \frac{Q_{inj} - (i-1)\frac{Q_{inj}}{Nz_{scr}} + Q_{recirc}}{\frac{Q_t^{in}}{Nz_{scr}} + Q_{inj} - (i-1)\frac{Q_{inj}}{Nz_{scr}} + Q_{recirc}} \quad \text{(A-13)}$$

Equation A-13 means that the stabilized concentration for each cell i depends on the stabilized concentration of the upper cell (i-1). This implies that the tracer concentration progressively declines along the screened interval. Using Equation A-13, it is therefore possible to predict the profile of stabilized concentrations along the screen depending on the recirculation flow rate. Then, the ratio $R_{b/t}$ (between the stabilized tracer concentration at the bottom of the tested interval $C_{w,stab,Nz}$ and the stabilized tracer concentration at the top of the tested interval $C_{w,stab,Nz-Nz_{scr}+1}$) can be calculated by integrating the Equation A-13 along the total length of the tested interval, which leads to the Equation 16 presented in the main manuscript.

References

Bear, J.: Dynamics of fluids in porous media, Courier Corporation, New York, NY, 764 pp., 1972.

Brouyère, S.: Etude et modélisation du transport et du piégeage des solutés en milieu souterrain variablement saturé. Evaluation des paramètres hydrodispersifs par la réalisation et l'interprétation d'essais de traçage in situ (study and modelling of transport and retardation of solutes in variably saturated media) (French. Ph.D. Thesis), University of Liège, Faculty of Applied Sciences, 2001.

Brouyère, S.: Modeling tracer injection and well-aquifer interactions: A new mathematical and numerical approach, Water Resour. Res., 39, https://doi.org/10.1029/2002WR001813, 2003.

Brouyère, S., Carabin, G., and Dassargues, A.: Influence of injection conditions on field tracer experiments, Ground Water, 43, 389–400, https://doi.org/10.1111/j.1745-6584.2005.0041.x, 2005.

Brouyère, S., Batlle-Aguilar, J., Goderniaux, P., and Dassargues, A.: A new tracer technique for monitoring groundwater fluxes: The Finite Volume Point Dilution Method, J. Contam. Hydrol., 95, 121–140, https://doi.org/10.1016/j.jconhyd.2007.09.001, 2008.

Dassargues, A.: Hydrogeology: Groundwater Science and Engineering, CRC Press, 2018.

Drost, W., Klotz, D., Koch, A., Moser, H., Neumaier, F., and Rauert, W.: Point dilution methods of investigating ground water flow by means of radioisotopes, Water Resour. Res., 4, 125–146, https://doi.org/10.1029/WR004i001p00125, 1968.

Dujardin, J., Anibas, C., Bronders, J., Jamin, P., Hamonts, K., Dejonghe, W., Brouyère, S., and Batelaan, O.: Combining flux estimation techniques to improve characterization of groundwater–surface-water interaction in the Zenne River, Belgium, Hydrogeol. J., 22, 1657–1668, https://doi.org/10.1007/s10040-014-1159-4, 2014.

Fourar, M., Radilla, G., Lenormand, R., and Moyne, C.: On the non-linear behavior of a laminar single-phase flow through two and three-dimensional porous media, Advances in Water Resources, 27, 669–677, https://doi.org/10.1016/j.advwatres.2004.02.021, 2004.

Goderniaux, P., Brouyère, S., Gutierrez, A., and Baran, N.: Multi-tracer tests to evaluate the hydraulic setting of a complex aquifer system (Br,villes spring catchment, France), Hydrogeol. J., 18, https://doi.org/10.1007/s10040-010-0633-x, 2010.

Halevy, E., Moser, H., Zellhofer, O., and Zuber, A.: Borehole dilution techniques: A critical review, IAEA, International Atomic Energy Agency (IAEA), 1967.

Hall, S.: Single Well Tracer Tests in Aquifer Characterization, Ground Water Monit. Remediat., 13, 118–124, https://doi.org/10.1111/j.1745-6592.1993.tb00443.x, 1993.

Hatfield, K., Annable, M., Cho, J., Rao, P. S. C., and Klammler, H.: A direct passive method for measuring water and contaminant fluxes in porous media, J. Contam. Hydrol., 75, 155–181, https://doi.org/10.1016/j.jconhyd.2004.06.005, 2004.

Jamin, P. and Brouyère, S.: Monitoring transient groundwater fluxes using the Finite Volume Point Dilution Method, J. Contam. Hydrol., 218, 10–18, https://doi.org/10.1016/j.jconhyd.2018.07.005, 2018.

Jamin, P., Goderniaux, P., Bour, O., Le Borgne, T., Englert, A., Longuevergne, L., and Brouyère, S.: Contribution of the finite volume point dilution method for measurement of groundwater fluxes in a fractured aquifer, J. Contam. Hydrol., 182, 244–255, https://doi.org/10.1016/j.jconhyd.2015.09.002, 2015.

Jamin, P., Cochand, M., Dagenais, S., Lemieux, J.-M., Fortier, R., Molson, J., and Brouyère, S.: Direct measurement of groundwater flux in aquifers within the discontinuous permafrost

zone: an application of the finite volume point dilution method near Umiujaq (Nunavik, Canada), Hydrogeol. J., 28, 869–885, 2020.

Lagarias, J. C., Reeds, J. A., Wright, M. H., and Wright, P. E.: Convergence Properties of the Nelder–Mead Simplex Method in Low Dimensions, SIAM J. Optim., 9, 112–147, https://doi.org/10.1137/S1052623496303470, 1998.

Lewis, D. C., Kriz, G. J., and Burgy, R. H.: Tracer dilution sampling technique to determine hydraulic conductivity of fractured rock, Water Resour. Res., 2, 533–542, https://doi.org/10.1029/WR002i003p00533, 1966.

Novakowski, K., Bickerton, G., Lapcevic, P., Voralek, J., and Ross, N.: Measurements of groundwater velocity in discrete rock fractures, J. Contam. Hydrol., 82, 44–60, https://doi.org/10.1016/j.jconhyd.2005.09.001, 2006.

Novakowski, K. S., Lapcevic, P. A., Voralek, J., and Bickerton, G.: Preliminary interpretation of tracer experiments conducted in a discrete rock fracture under conditions of natural flow, \grl, 22, 1417–1420, https://doi.org/10.1029/95GL00569, 1995.

Pitrak, M., Mares, S., and Kobr, M.: A Simple Borehole Dilution Technique in Measuring Horizontal Ground Water Flow, Groundwater, 45, 89–92, https://doi.org/10.1111/j.1745-6584.2006.00258.x, 2007.

Poulsen, D. L., Cook, P. G., Simmons, C. T., McCallum, J. M., Noorduijn, S. L., and Dogramaci, S.: A constant rate salt tracer injection method to quantify pumped flows in long-screened or open borehole wells, Journal of Hydrology, 574, 408–420, https://doi.org/10.1016/j.jhydrol.2019.04.051, 2019.

Quinn, P. M., Cherry, J. A., and Parker, B. L.: Quantification of non-Darcian flow observed during packer testing in fractured sedimentary rock, Water Resources Research, 47, https://doi.org/10.1029/2010WR009681, 2011.

West, L. J. and Odling, N. E.: Characterization of a Multilayer Aquifer Using Open Well Dilution Tests, Groundwater, 45, 74–84, https://doi.org/10.1111/j.1745-6584.2006.00262.x, 2007.

Wildemeersch, S., Jamin, P., Orban, P., Hermans, T., Klepikova, M., Nguyen, F., Brouyère, S., and Dassargues, A.: Coupling heat and chemical tracer experiments for estimating heat transfer parameters in shallow alluvial aquifers, Sel. Pap. 8th Int. Assoc. Hydrol. Sci. IAHS Groundw. Qual. Conf. 2013 GQ13 - Manag. Groundw. Qual. Support Compet. Hum. Ecol. Needs, 169, 90–99, https://doi.org/10.1016/j.jconhyd.2014.08.001, 2014.